pared with DMD. However, this hypothesis has not been verified.

Regeneration of skeletal muscle depends on the competence of muscle satellite cells. Muscle satellite cells, which account for 2 to 5% of the total nuclei in adult skeletal muscle, play a major role in muscle regeneration.[11] Under normal conditions, satellite cells are found external to the myofiber plasma membrane and beneath the muscle basal lamina,[12] and they are mitotically quiescent in adult skeletal muscle.[13] When activated by muscle damage, satellite cells proliferate, differentiate, fuse with each other or injured myofibers, and eventually regenerate mature myofibers. During the regenerative processes, satellite cells not only produce large amounts of muscle, but also renew themselves to maintain their own population.[14] In fact, it is reported that the satellite cell pool of C57BL/10 continues to respond efficiently even when the skeletal muscle is subjected to as many as 50 cycles of severe damage.[15] Therefore, it is thought that maintenance of the satellite cell pool is indispensable to retain the long-term regenerative potential for skeletal muscle injury, including in muscular dystrophies.

To investigate genetic differences in long-term regeneration potential, we first induced repeated degeneration–regeneration cycles in four inbred strains of mice. Among these strains, C57BL/6, a widely used strain akin to C57BL/10, was tolerant of repeated injury. This is consistent with the results of C57BL/10 previously described.[15] In contrast, among four inbred strains, DBA/2 mice exhibited the most remarkable skeletal muscle loss and impaired regeneration after repeated injury. Importantly, the self-renewal potential of DBA/2 satellite cells was significantly lower than that of C57BL/6. In addition, *in vitro* colony formation and proliferation assays indicated that intrinsic difference between C57BL/6 and DBA/2 satellite cells exist. Finally, we crossed the *mdx* genotype with the DBA/2 for more than five generations. At the fifth backcross, the mice are not yet fully congenic (D2.B10-*DMD*^{mdx}), and thus we refer to them as DBA/2-*mdx* hereafter. We investigated their phenotypes. Intriguingly, severe loss of skeletal muscle weight, decreased myofiber number, increased fat and fibrosis volume, and apparent muscle weakness were observed in the DBA/2-*mdx* mice. These results indicate that the intrinsic genetic program affects the properties of satellite cells, and DBA/2-*mdx* will be a more useful model of DMD than C57BL/10-*mdx*. It is also speculated that the high self-renewal potential of C57BL/10 satellite cells might explain the difference in pathologies between humans and mice.

Materials and Methods

Mice

Six-week-old, specific pathogen-free, BALB/c, C3H/HeN, C57BL/6, and DBA/2 mice were purchased from Charles River Japan (Yokohama, Japan). Six-week-old, specific pathogen-free C57BL/10 mice were purchased from Shimizu Laboratory Supplies Co., Ltd (Kyoto, Japan). Specific pathogen-free *mdx* mice (of C57BL/10 background) were provided by Central Laboratories of Experimental Animals (Kanagawa, Japan) and maintained in our animal facility by brother-sister matings. *Mdx* of C57BL/10 background were backcrossed into DBA/2 genetic background. Mice backcrossed more than five generations were used in this study. Genotyping was performed according to previous reports.[16] All procedures for experimental animals were approved by the Experimental Animal Care and Use Committee at Osaka University.

Muscle Injury

Muscle injury was induced by injecting cardiotoxin (10 μmol/L in saline, Wako Pure Chemical Industries, Tokyo, Japan) into tibialis anterior (50 μl), gastrocnemius (150 μl), and quadriceps femoris (100 μl) muscles as described.[17] All injections were first done when mice were 8 to 10 weeks of age.

Histological Analysis

Tibialis anterior, gastrocnemius, and quadriceps femoris muscles were isolated and frozen in liquid nitrogen-cooled isopentane (Wako Pure Chemical Industries). Cryosections (10 μm) were stained with H&E, Oil red-O (Sigma-Aldrich, St. Louis, MO), or Sirius Red (Sigma-Aldrich).

Immunohistochemistry

For immunohistochemical examinations, transverse cryosections (6 μm) were stained with various antibodies. Monoclonal rat anti-laminin α2 (1:200; clone: 4H8-2) and mouse anti-Pax7 antibodies were purchased from Alexis Biochemical (Lausen, Switzerland) and Developmental Studies Hybridoma Bank (Iowa, IA), respectively. For Pax7 staining, a M.O.M. kit (Vector Laboratories, Burlingame, CA) was used to block endogenous mouse IgG. After the first staining at 4°C overnight, sections were reacted with secondary antibodies conjugated with Alexa 488 or Alexa 568 (Molecular Probes, Eugene, OR). Sections were shielded using Vectashield (Vector Laboratories, Inc). The signals were recorded photographically using an Axiophot microscope (Carl Zeiss, Oberkochen, Germany).

Preparation of Muscle Satellite Cells and Culture

Satellite cells were isolated from uninjured adult skeletal muscle using biotinylated-SM/C-2.6[18] and IMag methods (BD Immunocytometry Systems, Mountain View, CA) as described in a previous report.[17] Satellite cells were cultured in a growth medium of high-glucose Dulbecco's modified Eagle's medium (Sigma-Aldrich) containing 20% fetal calf serum (Trace Biosciences, N.S.W., Australia), 2.5 ng/ml basic fibroblast growth factor (PeproTech, London, UK), leukemia inhibitory factor (Alexis Biochemical), and penicillin (100 U/ml)-streptomycin

(100 μg/ml) (Gibco BRL, Gaithersburg, MD) on culture dishes coated with Matrigel (BD Bioscience, San Diego, CA).

Colony Forming Assay

Clonal cultures of freshly isolated satellite cells were performed in 96-well plates coated with type I collagen (Sumilon, Tokyo, Japan) in growth medium for a week. The frequency of colony formation and number of cells in each well were counted under a phase-contrast microscope.

Cell Proliferation Assay

Isolated satellite cells were cultured in growth medium for 3 to 4 days, and expanded primary myoblasts were harvested and additional culture was performed in 96-well dishes for 1 day. Eight hours later, bromodeoxyuridine (BrdU) uptake was quantified using the Cell Proliferation ELISA, BrdU Kit (Roche Diagnostics, Basel, Switzerland) and a microplate reader (Model 680, Bio-Rad, Hercules, CA).

Measurement of Sizes of Myofibers and Oil Red-O-Positive and Fibrotic Areas

Image J software was used to measure myofiber sizes and Oil red-O- and Sirius Red-positive areas.

Evans Blue Dye Injection

Evans blue (Wako Pure Chemical Industries) was dissolved in PBS and injected intraperitoneally into mice (1 mg/100 μl/10g body weight).[19] Sixteen to 18 hours later, muscle tissues were removed, and frozen in liquid nitrogen-cooled isopentane. The muscle fibers with Evans Blue incorporated were then counted as injured muscles.

Muscle Endurance and Grip Strength Test

The muscle endurance test was referred to the studies by Handschin et al.[20] In brief, we used a MK-680S treadmill (Muromachi Kikai Co., Ltd., Tokyo, Japan). For 3 days, animals were acclimated to treadmill running for 5 minutes at a speed of 10 m/min on a 0% grade. After the acclimation, animals ran on a treadmill with a 10% uphill grade starting at a speed of 10 m/min for 5 minutes. Every subsequent 2 minutes, the speed was increased by 2 m/min until the mice were exhausted. Exhaustion was defined as the inability of the animal to remain on the treadmill despite mechanical prodding. Running time and speed were measured, and the distance was calculated. Grip strength was measured using a MK-380M grip strength meter (Muromachi Kikai Co., Ltd). The grip strength of each individual mouse was measured 10 times, the same measurements were repeated on the next day, and the highest value of each experiment was used.

Statistics

Values were expressed as means ± SD. Statistical significance was assessed by Student's *t*-test. In comparisons of more than two groups, nonrepeated measures analysis of variance (analysis of variance) followed by the Student-Newman-Keuls test were used. A probability of less than 5% ($P < 0.05$) or 1% ($P < 0.01$) was considered statistically significant.

Results

Genetic Differences in Skeletal Muscle Regeneration

To examine the long-term regeneration ability of four inbred strains of mice, repeated cycles of degeneration–regeneration were induced by injection of cardiotoxin (CTX). CTX was injected into one side of the tibialis anterior (TA), gastrocnemius (GC), and quadriceps (Qu) muscle every 2 weeks. At the last (sixth) CTX injection, another intact TA muscle received CTX once to examine the regenerative potential in one cycle of each mouse at this age. Four weeks later, the muscles were removed and analyzed. As shown in Figure 1, A and B, none of the strains displayed a striking difference in either skeletal muscle weight or histochemistry after one CTX injection (CTX-1), except for the appearance of adipocytes in BALB/c. However, the DBA/2 mice that received six CTX injections (CTX-6) exhibited remarkably impaired regeneration (Figure 1A) and loss of TA muscle weight (Figure 1B). A similar loss of muscle weight was also observed in GC and Qu of DBA/2 (CTX-6 in Figure 1C). In contrast, none of the other strains showed a significant difference in uninjured muscle weight at this age (uninjured in Figure 1C). Fat was observed in DBA/2, BALB/c, and C3H/HeN after six injections, but the sclerosis and loss of muscle weight was remarkable in DBA/2. Therefore, the following experiments were performed on C57BL/6 and DBA/2.

Regeneration Impairment in DBA/2 Is Inherited Recessively

To assess the inheritance of the lower regeneration ability of DBA/2, we injected CTX into C57BL/6, DBA/2, and their F1 mice (B6D2F1). To allow more sufficient regeneration time, the interval between CTX injections was changed to 4 weeks. As shown in Figure 2A, we found marked muscle weight loss in DBA/2 after three CTX injections (4 weeks × 3). The results of B6D2F1 mice were similar to those of C57BL/6 (Figure 2, A and B).

As shown in Figure 1A, DBA/2 mice exhibited impaired regeneration accompanied by accumulation of fat and fibrosis after three CTX injections (4 weeks × 3), but not in the 4 weeks × 1 experiment (Figure 2B). Oil red-O (Figure 2C) and Sirius Red (Figure 2D) stainings were performed to determine the amount of fat and fibrosis, respectively. As shown in Figure 2E, increments in fat and fibrotic areas were observed in DBA/2 mice receiving

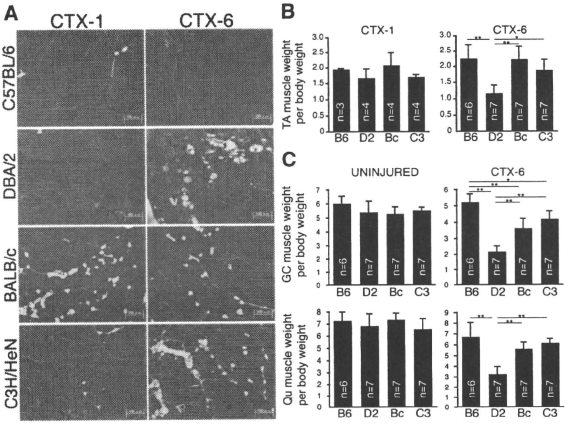

Figure 1. Impaired regeneration and loss of muscle weight in DBA/2 mice after injured six times. **A:** TA (tibialis anterior) muscles were examined histologically in four inbred strains of mice after one (CTX-1) or six (CTX-6) cardiotoxin (CTX) injections. The cross sections were stained with H&E. Scale bar = 100 μm. **B:** The TA muscle weight (mg) per body weight (g) in each inbred strain after one or six CTX injections. B6, D2, Bc, and C3 indicate C57BL/6, DBA/2, BALB/c, and C3H/HeN mice, respectively. **C:** The GC (gastrocnemius) and Qu (quadriceps) muscle weights (mg) per body weight (g) in each inbred strain from uninjured or muscle injured six times. The number in the each graph indicates the number of mice used in these experiments. $^{*}P < 0.05$, $^{**}P < 0.01$ (analysis of variance, SNK-test).

three injections (4 weeks × 3). In 4 weeks × 1 DBA/2, the fat accumulation of one mouse was a slightly higher volume (2.02%), but three mice showed little fat accumulation (less than 0.6%). In contrast to DBA/2, C57BL/6, and B6D2F1 mice did not show any sign of impaired regeneration. These results indicate that the impaired regeneration ability of the DBA/2 strain after repeated injury is recessive heredity.

Loss of Muscle Mass Results from Decreased Number and Size of Myofibers

To assess the cause of muscle weight loss in DBA/2, the numbers and sizes of myofibers were quantified. In uninjured muscle, no significant difference between the numbers of myofibers was observed in C57BL/6 and DBA/2 (Figure 3A). However, as shown in Figure 3B, decreased numbers of myofibers were observed in DBA/2 after three CTX injections (4 weeks × 3), as compared with 4 weeks × 1 or uninjured muscle. C57BL/6 showed more myofibers than uninjured muscle after one or three injections (Figure 3B).

The sizes of myofibers were also measured. Four weeks after one CTX injection (4 weeks × 1), the size of myofibers in DBA/2 was similar to that in C57BL/6 (Figure 3, C and D). However, the regenerated myofibers of DBA/2 (4 weeks × 3) were slightly smaller than those of C57BL/6 (Figure 3, C and D). These data indicate that the loss of muscle weight in DBA/2 results from the decreased number and size of myofibers.

Decreased Number of Self-Renewed Satellite Cells in DBA/2

We hypothesized that a decreased number of satellite cells leads to the loss of myofibers, because myofibers are mainly made by satellite cells. To elucidate this hypothesis, we examined the number of satellite cells. As shown in Figure 3E, cells positive for Pax7, a specific marker of satellite cells,[21] lying beneath the basal lamina were counted. There was no significant difference between the uninjured TA muscles of C57BL/6 and DBA/2 mice. However, a remarkable decrease in the number of satellite cells was observed in DBA/2 after three CTX injections (Figure 3F). These results imply that the functions (including self-renewal potential) of satellite cells include responsibility for most of the regeneration of impaired muscle in DBA/2.

Colony Formation and Proliferation of Satellite Cells from DBA/2

To examine whether there is an intrinsic difference between the satellite cells of C57BL/6 and DBA/2, satellite cells were isolated and cultured *in vitro*. As shown in Figure 4A, the BrdU uptake of primary myoblasts of DBA/2 was inferior to that of C57BL/6 myoblasts. Next, we performed a colony-forming assay of single satellite cells. As shown in Figure 4C, single DBA/2 satellite cell did not produce large colonies similar to those of C57BL/6. The frequencies of colony forming cells did not differ in C57BL/6 and DBA/2 (Figure 4B). These results indicate that intrinsic factors affect the properties of satellite cells.

*Loss of Muscle Weight in DBA/2-*mdx

To assess whether the low regenerative potential of mice with the dystrophin mutation exhibit DMD-like features, we crossed C57BL/10-*mdx* (B10-*mdx*) into DBA2. It was reported that body weight of B10-*mdx* is heavier than that of the control wild-type.[22] In contrast to B10-*mdx*, DBA/

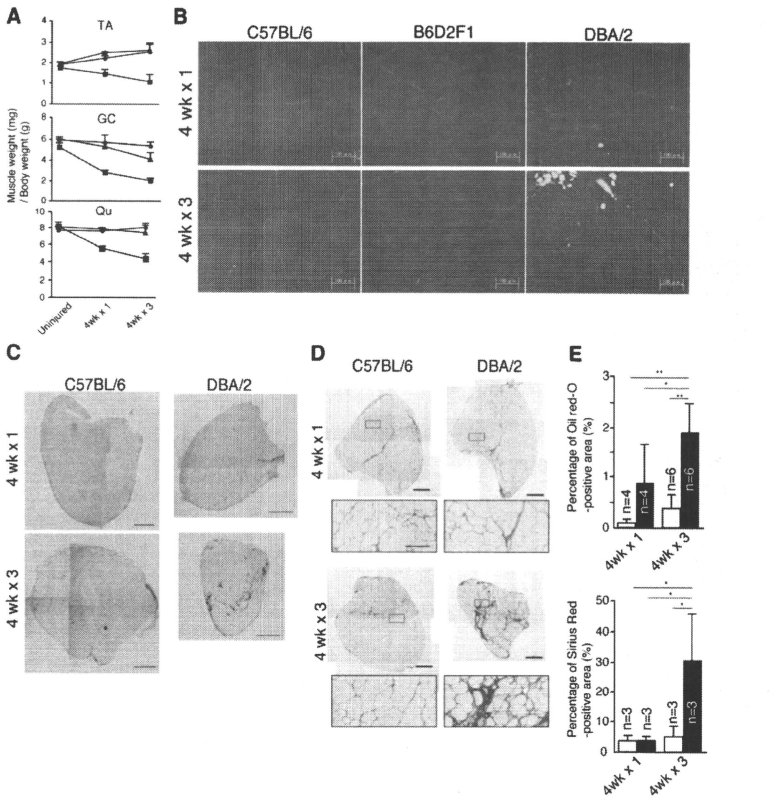

Figure 2. Impaired regeneration of DBA/2 phenotype is recessively inherited. **A:** The TA, GC, and Qu muscle weights (mg) per body weight (g) in C57BL/6 (closed circles), DBA/2 (closed squares), and B6D2F1 (closed triangles) mice after one (4 weeks × 1) or three CTX injections (4 weeks × 3). The cross sections were stained with H&E (**B**), Oil red-O (**C**), or Sirius Red (**D**). Scale bars: 100 μm (**B**); 500 μm (**C** and **D**). **E:** The *y* axis shows the mean percentage of Oil red-O or Sirius Red-positive areas per section. White and black columns indicate the results of C57BL/6 and DBA/2, respectively. The number in the each graph indicates the number of mice used in this analysis. $^{*}P < 0.05$, $^{**}P < 0.01$ (analysis of variance, SNK-test).

2-*mdx* (D2-*mdx*) mice showed the decreased body weight regardless of gender (Figure 5A). A more remarkable phenotype of D2-*mdx* was the loss of skeletal muscle mass (Figure 5B). As previously reported, the muscle weight of B10-*mdx* was heavier than that of controls,[8] but the TA, GC, and Qu muscle weights of D2-*mdx* males were 71%, 59%, and 54% of those of controls, respectively (Figure 5C). Female muscles were 85% (TA), 61% (GC), and 52% (Qu) of each control muscle, respectively. The loss of muscle weight did not simply reflect the decreased body weight because there is also a significant difference in muscle weight (mg) per body weight (g) between D2-*mdx* and control littermates (Figure 5C). Control littermates of D2-*mdx* and normal DBA/2 exhibited similar results in muscle weight per body weight ratios (data not shown).

Histology of DBA/2-mdx

In contrast to the histology of DMD, it is widely accepted that fibrosis and fat replacement are minimal in B10-*mdx*.[7] In addition, there was no apparent fiber loss. To examine the accumulation of fibrosis and fat tissue in D2-*mdx*, cross sections were stained with Sirius Red or Oil red-O. As shown in Figure 6, A and B, there was no sign of fibrosis or adipogenesis in B10-*mdx*. However, D2-*mdx* mice exhibited increased fibrosis and fat accu-

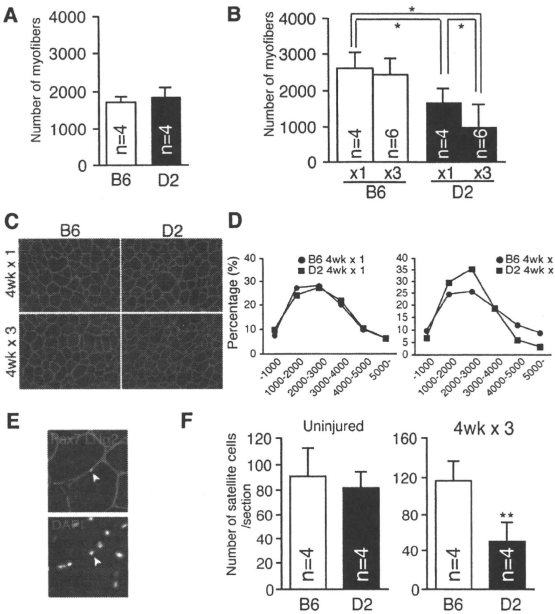

Figure 3. Decreased numbers of myofibers and satellite cells in DBA/2 mice after three repeated injuries. **A:** The number of myofibers in uninjured TA muscle at 10 weeks old. The *y* axis shows the mean number of myofibers per section. B6 and D2 indicate C57BL/6 and DBA/2, respectively. **B:** The mean numbers of myofiber in TA muscles after one or three injuries. $^{*}P < 0.05$ (analysis of variance, SNK-test). The sizes of myofibers in TA muscle after one or three CTX injections. **C:** Cross sections were stained with anti-laminin α2 antibody (green). **D:** The size of each myofiber in TA muscle was measured after one or three injections. Closed circles or squares show the results of C57BL/6 or DBA/2, respectively. **E: Arrowhead** indicates Pax7 expressing cells lying beneath the basal lamina. **F:** The number of satellite cells in noninjured TA muscle (uninjured) or TA muscle injured three times (4 weeks × 3). The *y* axis shows the mean number of satellite cells per section. The number in each graph indicates the number of mice used in these analyses. $^{**}P < 0.01$ (Student's *t*-test).

mulation in comparison with B10-*mdx*. In contrast to B10-*mdx*, a decreased number of total myofibers was also observed in D2-*mdx* (Figure 6C).

To enumerate the number of necrotic fibers, the mice were injected with Evans blue dye to visualize necrotic fibers. As shown in Figure 6C, fewer total necrotic fibers were observed in D2-*mdx*. This result suggests that the D2-*mdx* phenotype does not result from acceleration of degeneration.

Decreased Skeletal Muscle Function in DBA/2-mdx

Skeletal muscle endurance was assessed by treadmill running to exhaustion as an indicator of maximal muscle capacity. After acclimatization, mice were run on a 10% slope at increasing speed until the animals were unable to remain on the treadmill despite prodding. We then recorded the end time and speed to calculate the distance run. As shown in Figure 7A, male and female D2-*mdx* ran 45% and 56% shorter distances than control littermates. The maximum speed of D2-*mdx* was also lower than that of their littermate. The distance run showed the most significantly difference because of the protocol of increasing speed (Figure 7A). The average distance run by male controls was 544 meters, but that of D2-*mdx* males was 205 meters (38% of the control). A similar result was shown by female D2-*mdx* (25% of the control). B10-*mdx* also showed lower values compared with normal C57BL/10 mice (data not shown), but the decreased ratio of each parameter in D2-*mdx* was more remarkable than that in B10-*mdx* (Figure 7B).

A grip strength test was also performed as an indicator of motor function and whether D2-*mdx* exhibited muscle weakness compared with controls. As shown in Figure 7C, D2-*mdx* earned a lower score than control mice regardless of gender. However, there was no significant difference between B10-*mdx* and control mice.

Discussion

Repeated Injury Models

Muscle satellite cells play central roles in skeletal muscle regeneration.[23] Satellite cells produce a vast number of progenitor cells (myoblasts) that finally become myofibers. During this process, at least some of the satellite cells have self-renewal potential,[14,24] but are quiescent and will respond efficiently to the next damages. In fact, Luz et al[15] indicated that C57BL/10 could regenerate after 50 bupivacaine injections without the loss of myofibers or gain of fibrotic areas in the TA muscle. Importantly, C57BL/10-*mdx* mice exhibited decreased numbers of myofibers after 50 bupivacaine injections[15]

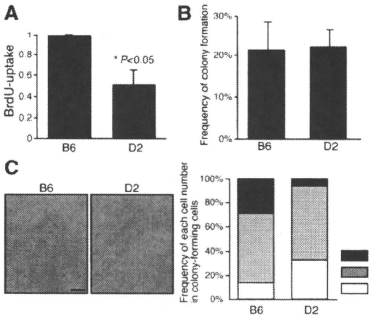

Figure 4. Satellite cells of DBA/2 strain show inferior BrdU uptake and colony-forming potential. **A:** BrdU uptake of primary myoblasts derived from C57BL/6 or DBA/2 satellite cells. The *y* axis shows the mean with SD of three independent experiments. $^{*}P < 0.05$ (Student's *t*-test). Frequency of colony formation by a single satellite cell derived from C57BL/6 or DBA/2 (**B**) and the size of single cell-derived colonies (**C**). The picture shows representative colonies of each strain. Colonies were categorized into three groups: >50 cells/well, 10 to 49 cells/well, and 2 to 9 cells/well. The *y* axis indicates the frequency (**B**) or percentage of each category (**C**) from three independent experiments. Scale bar = 100 μm.

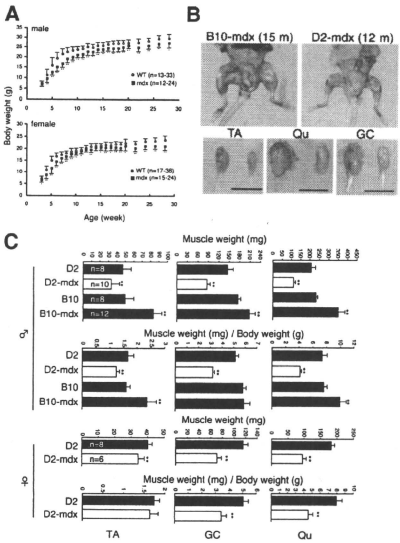

Figure 5. DBA/2-*mdx* mice show decreased body weight and remarkable muscle weight loss. **A:** Body weight of D2-*mdx* (closed squares) and their wild or heterozygous littermates (open circles) related to age. $^{*}P < 0.05$, $^{**}P < 0.01$ (Student's *t*-test) **B:** Photographs of hind limb muscles of male B10-*mdx* (15 months) and D2-*mdx* (12 months). Scale bar = 1 cm. **C:** TA, GC, and Qu muscle weights (mg) or per body weight (g) of 6-month-old mice. *x* axis shows the mean with SD. The numbers of muscles used in each study are shown in each graph. $^{*}P < 0.05$, $^{**}P < 0.01$.

because C57BL10-*mdx* mice already have dystrophic degeneration–regeneration cycles. Sadeh et al[25] also showed active regeneration cycles in rats that received weekly injections of bupivacaine for 6 months. They reported that there was lack of evidence for reduction or exhaustion of muscle fiber capacity to regenerate despite ongoing degeneration–regeneration over a period approximating one fourth of the rat life expectancy. These results indicate that the satellite cell pool was efficiently maintained for multiple degeneration–regeneration cycles in these animals, and that dystrophic mice exhibit less regeneration ability. However, DBA/2 showed significantly decreased numbers of myofibers and self-renewed satellite cells after only three injections of CTX.

The number of DBA/2 satellite cells in uninjured TA muscle is similar to that of C57BL/6. Although, the myofibers in DBA/2 were smaller than those in C57BL/6 2 weeks after one CTX injection (data not shown), the myofiber size and histological characteristics showed few significant differences between and DBA/2 and C57BL/6 4 weeks after a single CTX injection. These results suggest that the self-renewal ability of DBA/2 satellite cells is incomplete and that the exhaustion of muscle satellite cells leads to a decreased number of myofiber and loss of skeletal muscle weight. Nonmyogenic cells, for example, macrophages, also play important roles in skeletal muscle regeneration. However, dysfunction of macrophages leads to impaired regeneration after one CTX injection.[26,27] Furthermore, the remarkable regeneration deficit was not observed in DBA/2 4 weeks after one CTX injection in TA muscle. These results suggest that repeated injury is a suitable model to assess the long-term regeneration potential of skeletal muscle, and that the self-renewal ability of satellite cells is responsible at least in part for the result of repeatedly injured muscle in DBA/2.

Strain Differences of Muscle Regeneration Ability

C57BL/6, a strain akin to C57BL/10, is the most widely used strain for skeletal muscle regeneration studies. As shown in Figure 1, C57BL/6 has the best ability to regenerate skeletal muscle among the four inbred strains examined. An early study by Grounds and McGeachie[28] indicated a strain difference in skeletal muscle regeneration between BALB/c and Swiss SJL/J. They showed that superior and faster regeneration was observed in the Swiss SJL/J strain. The most outstanding phenotype of DBA/2 is the remarkable decrease of muscle weight compared with the three other inbred strains, including BALB/c. Intriguingly, DBA/2 mice have a shorter life span than C57BL/6.[29] In addition, it is reported that muscle weight loss is increased during aging (sarcopenia) in DBA/2 mice compared with C57BL/6.[30] The reason why the DBA/2 strain exhibits the loss of muscle weight is unknown, but our results imply a relationship between

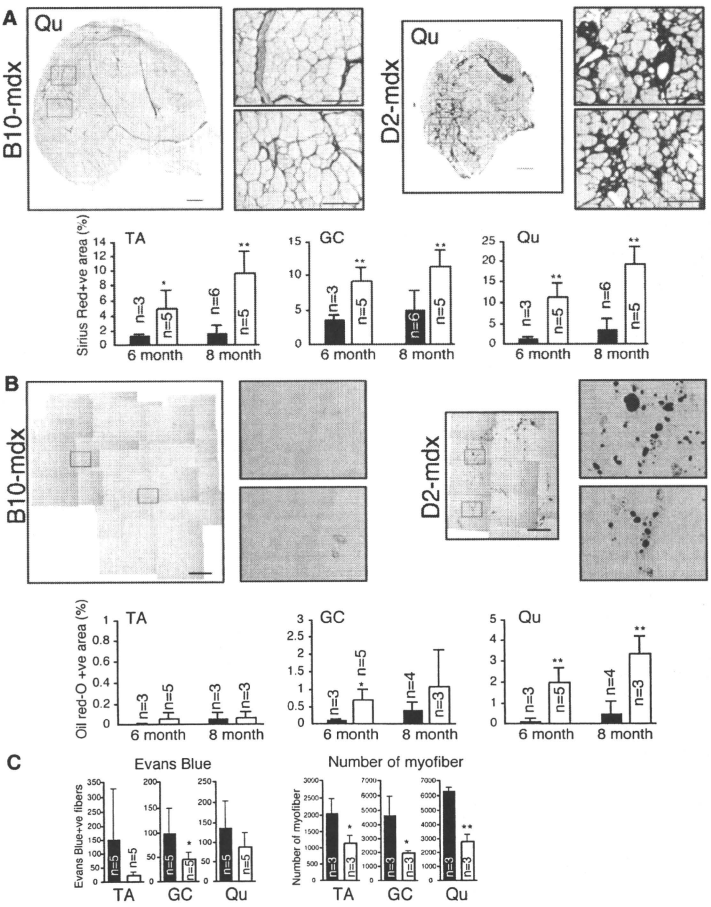

Figure 6. Histological analyses of DBA/2-*mdx* mice. Sirius red staining (**A**) and Oil red-O staining (**B**) of Qu muscle of 8-month-old B10-*mdx* and D2-*mdx* mice. The *y* axis indicates the mean percentage of Sirius Red- (**A**) or Oil red-O (**B**) -positive areas per section. The *x* axis indicates the age of mice. Black and white columns show the results for B10-*mdx* and D2-*mdx*, respectively. The numbers of mice used in each study are shown in each graph. **C:** The *y* axis indicates the mean number of Evans blue-positive or total myofibers of B10-*mdx* and D2-*mdx* at 8 months of age. $^{*}P < 0.05$, $^{**}P < 0.01$.

the impaired function of satellite cells and sarcopenia in DBA/2.

Heydemann et al[31] reported that γ-sarcoglycan-null mice with DBA/2 background showed decreased skeletal muscle weight, increased Evans Blue uptake, and a higher hydroxyproline concentration than C57BL/6, CD1, and 129 background null mice. Although they ruled out the voluntary activities of DBA/2, they did not discuss the cause of these results. Our results suggest that the low regeneration potential of DBA/2 leads to a severe skeletal muscle phenotype in various dystrophic mouse models.

The DBA/2J strain has been used in sarcopenia and γ-sarcoglycan-null mouse studies.[30,31] To exclude the possibility that DBA/2 substrain differences exist, we compared the BrdU uptake of primary myoblasts in DBA/2N (used in this study) and DBA/2J. Because we observed similar low BrdU uptakes by primary myoblasts in both DBA/2N and DBA/2J (data not shown), these

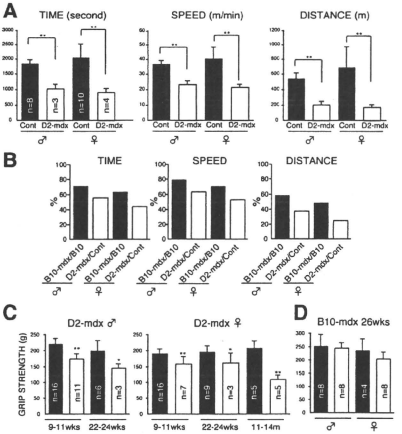

Figure 7. Comparison of muscle strength in DBA/2-*mdx* and B10-*mdx*. **A:** Treadmill running test of mice at 24 weeks old. Final time, speed, and distance were recorded and calculated for the individual performance score. The averages are shown with SD. Control indicates heterozygous or wild-type littermates of D2-*mdx*. The numbers of mice used in each study are shown in each graph. $^{*}P < 0.05$, $^{**}P < 0.01$. **B:** Comparison of C57BL/10-*mdx* and DBA/2-*mdx* in treadmill running test. The *y* axis indicates the percentage of *mdx* per control value. The numbers of male C57BL/10, male C57BL/10-*mdx*, female C57BL/10, and female C57BL/10-*mdx* are 4, 4, 4, and 8, respectively. Grip strength test of D2-*mdx* (**C**) or B10-*mdx* (**D**). Black and white columns indicate the results for *mdx* or control mice, respectively. The *y* axis indicates the average score of each mouse with SD. The *x* axis shows the ages of mice. The number in the each graph indicates the number of mice taking this test. $^{*}P < 0.05$, $^{**}P < 0.01$.

results suggest that lower muscle regeneration is common to the DBA/2 strain.

Stem (Satellite) Cell Function and Mouse Strains

As mentioned above, some previous reports indicated different responses in skeletal muscle regeneration among inbred strains of mice. However, to our knowledge, this is the first evidence that there is an intrinsic difference in satellite cells among inbred mice. The exact relationship between *in vitro* and *in vivo* results of satellite cells is not clear. However, low or slow proliferation of satellite cells might explain the decreased muscle weight and slow regeneration after a single injury in DBA/2 in comparison with C57BL/6 and B6D2F1, which showed increased muscle weight in their TA muscle (Figure 2A). It is unlikely that telomere erosion contributes to the *in vitro* and *in vivo* results of DBA/2 satellite cells because DBA/2 mice have longer telomeres than C57BL/6 mice.[32]

Recently Kuang et al[33] reported that satellite cells are a heterogeneous population of stem cells (satellite stem cells) and committed progenitor cells, and that they can be distinguished from others by Myf5 expression. They showed that Myf5-negative (satellite stem) cells self-renewed three times more frequently than Myf-5-positive (progenitor) cells *in vivo*. Schultz and Lipton[34] first described the heterogeneity of satellite cells by the different colony sizes of each satellite cell and found decreased colony sizes in aging muscle in the rat. Although it was not determined whether satellite stem cells form a large-colonies or not *in vitro*, our results showed that mice having low self-renewing satellite cells (DBA/2) exhibit smaller colony formations than mice having high self-renewing satellite cells (C57BL/6). These results suggest that satellite stem cells may form larger colonies *in vitro*.

In contrast to satellite cells, a highly strain-dependent function of hematopoietic stem cells was reported.[35] Chen et al[36] reported that DBA/2 showed a decline in primitive hematopoietic stem cell function with age, but that it increased with age in C57BL/6 in a *vivo* transplantation study. Recombinant inbred mice, named BXD strains, are available. Using BXD, Liang et al[37] identified latexin as affecting the size of the hematopoietic stem cell population in mice. A similar approach might lead to the discovery of key genes that affect the properties of satellite cells.

DBA/2-mdx *as Model for DMD*

Mdx was discovered a quarter of a century ago.[5] In 1989, the *mdx* mutation, a C to T transition within exon 23, was identified in the dystrophin gene on the X chromosome.[38] Nearly all *mdx* colonies are maintained as homozygous inbred lines; in addition, the difficulty of point mutation typing might impede the effect of genetic background on *mdx* phenotype. However, Amalfitano and Chamberlain[16] reported a rapid and simple typing strategy, and we established DBA/2-*mdx* following their protocol. C57BL/10-*mdx* mice have played central roles in a vast array of pathological, clinical, and physiological studies as a model for DMD. However, they do not reflect human pathology in some aspects, including little fat and fibrosis accumulation, no loss of myofiber numbers, and muscle weight. Recently, Gargioli et al[39] showed that the advanced stage of dystrophy including sclerosis precluded treatment by stem cell therapy. Therefore, assessment of therapeutic effect in more severe disease conditions is needed.

In marked contrast to the severe phenotype observed in DMD, early studies using C57BL/10-*mdx* concluded that they do not show obvious functional disability.[5,7] However, some later reports indicated functional differences between C57BL/10-*mdx* and control mice.[40–43] As shown in Figure 7, C57BL/6-*mdx* also showed muscle weakness in the treadmill test. However, the muscle weakness of DBA/2-*mdx* is more remarkable than that of C57BL/10-*mdx*. Therefore, DBA/2-*mdx* is a more appropriate model to assess skeletal muscle function after therapeutic treatment.

Chamberlain et al[44] reported that the average life spans of female and male C57BL/10-*mdx* mice were 22.5 and 21.5 months, respectively. Pastoret et al[8] also reported that C57BL/10-*mdx* mice have short life spans and that C57BL/10-*mdx* older than 78 weeks exhibit progressive weakness. We have not determined the life span of DBA/2-*mdx*, but it will be clarified in the future. Intrigu-

ingly, Chamberlain et al[44] observed the appearance of rhabdomyosarcoma-like tumors in C57BL/10-*mdx*. They speculate that the lifelong continuous myofiber degeneration and regeneration that characterize this animal model are associated with continuous and massive activation and proliferation of satellite cells, which greatly increase the chance of developing random and spontaneous mutations. To date, we have observed tumors in C57BL/10-*mdx* but not in DBA/2-*mdx*. This observation supports their speculations.

The reasons why *mdx* mice do not show the human-like pathology have been investigated. One reason for the difference between DMD and *mdx* is explained by the presence of utrophin, a homolog of dystrophin. Utrophin is located in the neuromuscular junction in normal muscle. In dystrophic muscle, utrophin is up-regulated in the sarcolemma and compensates for dystrophin function. As shown in Figure 6, the results of Evans blue uptake in DBA/2-*mdx* indicated that the degeneration of myofiber was not accelerated, but that the regeneration potential was inferior. These results clearly indicate that not only utrophin expression but also regeneration potential, perhaps a satellite cell function, directly leads to the pathological condition. The identification of genes that determine the DBA/2 phenotype will provide new therapeutic strategies for the treatment of muscular dystrophy.

Acknowledgment

We thank Katherine Ono for reading this manuscript.

References

1. Koenig M, Monaco AP, Kunkel LM: The complete sequence of dystrophin predicts a rod-shaped cytoskeletal protein. Cell 1988, 53:219–228
2. Suzuki A, Yoshida M, Hayashi K, Mizuno Y, Hagiwara Y, Ozawa E: Molecular organization at the glycoprotein-complex-binding site of dystrophin. Three dystrophin-associated proteins bind directly to the carboxy-terminal portion of dystrophin. Eur J Biochem 1994, 220:283–292
3. Ervasti JM, Campbell KP: A role for the dystrophin-glycoprotein complex as a transmembrane linker between laminin and actin. J Cell Biol 1993, 122:809–823
4. Carpenter S, Karpati G: Disease of skeletal muscle. Edited by S Carpenter, G Karpati. New York, Oxford University Press, Inc., 2001, pp. 373–524
5. Bulfield G, Siller WG, Wight PA, Moore KJ: X chromosome-linked muscular dystrophy (mdx) in the mouse. Proc Natl Acad Sci USA 1984, 81:1189–1192
6. Stedman HH, Sweeney HL, Shrager JB, Maguire HC, Panettieri RA, Petrof B, Narusawa M, Leferovich JM, Sladky JT, Kelly AM: The mdx mouse diaphragm reproduces the degenerative changes of Duchenne muscular dystrophy. Nature 1991, 352:536–539
7. Tanabe Y, Esaki K, Nomura T: Skeletal muscle pathology in X chromosome-linked muscular dystrophy (mdx) mouse. Acta Neuropathol 1986, 69:91–95
8. Pastoret C, Sebille A: mdx mice show progressive weakness and muscle deterioration with age. J Neurol Sci 1995, 129:97–105
9. Deconinck AE, Rafael JA, Skinner JA, Brown SC, Potter AC, Metzinger L, Watt DJ, Dickson JG, Tinsley JM, Davies KE: Utrophin-dystrophin-deficient mice as a model for Duchenne muscular dystrophy. Cell 1997, 90:717–727
10. Grady RM, Teng H, Nichol MC, Cunningham JC, Wilkinson RS, Sanes JR: Skeletal and cardiac myopathies in mice lacking utrophin and dystrophin: a model for Duchenne muscular dystrophy. Cell 1997, 90:729–738
11. Bischoff R: Analysis of muscle regeneration using single myofibers in culture. Med Sci Sports Exerc 1989, 21:S164–172
12. Mauro A: Satellite cell of skeletal muscle fibers. J Biophys Biochem Cytol 1961, 9:493–495
13. Schultz E, Gibson MC, Champion T: Satellite cells are mitotically quiescent in mature mouse muscle: an EM and radioautographic study. J Exp Zool 1978, 206:451–456
14. Collins CA, Olsen I, Zammit PS, Heslop L, Petrie A, Partridge TA, Morgan JE: Stem cell function, self-renewal, and behavioral heterogeneity of cells from the adult muscle satellite cell niche. Cell 2005, 122:289–301
15. Luz MA, Marques MJ, Santo Neto H: Impaired regeneration of dystrophin-deficient muscle fibers is caused by exhaustion of myogenic cells. Braz J Med Biol Res 2002, 35:691–695
16. Amalfitano A, Chamberlain JS: The mdx-amplification-resistant mutation system assay, a simple and rapid polymerase chain reaction-based detection of the mdx allele. Muscle Nerve 1996, 19:1549–1553
17. Fukada S, Yamamoto Y, Segawa M, Sakamoto K, Nakajima M, Sato M, Morikawa D, Uezumi A, Miyagoe-Suzuki Y, Takeda S, Tsujikawa K, Yamamoto H: CD90-positive cells, an additional cell population, produce laminin alpha2 upon transplantation to dy(3k)/dy(3k) mice. Exp Cell Res 2008, 314:193–203
18. Fukada S, Higuchi S, Segawa M, Koda K, Yamamoto Y, Tsujikawa K, Kohama Y, Uezumi A, Imamura M, Miyagoe-Suzuki Y, Takeda S, Yamamoto H: Purification and cell-surface marker characterization of quiescent satellite cells from murine skeletal muscle by a novel monoclonal antibody. Exp Cell Res 2004, 296:245–255
19. Matsuda R, Nishikawa A, Tanaka H: Visualization of dystrophic muscle fibers in mdx mouse by vital staining with Evans blue: evidence of apoptosis in dystrophin-deficient muscle. J Biochem 1995, 118:959–964
20. Handschin C, Chin S, Li P, Liu F, Maratos-Flier E, Lebrasseur NK, Yan Z, Spiegelman BM: Skeletal muscle fiber-type switching, exercise intolerance, and myopathy in PGC-1alpha muscle-specific knock-out animals. J Biol Chem 2007, 282:30014–30021
21. Seale P, Sabourin LA, Girgis-Gabardo A, Mansouri A, Gruss P, Rudnicki MA: Pax7 is required for the specification of myogenic satellite cells. Cell 2000, 102:777–786
22. Connolly AM, Keeling RM, Mehta S, Pestronk A, Sanes JR: Three mouse models of muscular dystrophy: the natural history of strength and fatigue in dystrophin-, dystrophin/utrophin-, and laminin alpha2-deficient mice. Neuromuscul Disord 2001, 11:703–712
23. Charge SB, Rudnicki MA: Cellular and molecular regulation of muscle regeneration. Physiol Rev 2004, 84:209–238
24. Sacco A, Doyonnas R, Kraft P, Vitorovic S, Blau HM: Self-renewal and expansion of single transplanted muscle stem cells. Nature 2008, 456:502–506
25. Sadeh M, Czyewski K, Stern LZ: Chronic myopathy induced by repeated bupivacaine injections. J Neurol Sci 1985, 67:229–238
26. Arnold L, Henry A, Poron F, Baba-Am Y, van Rooijen N, Plonquet A, Gherardi RK, Chazaud B: Inflammatory monocytes recruited after skeletal muscle injury switch into anti-inflammatory macrophages to support myogenesis. J Exp Med 2007, 204:1057–1069
27. Segawa M, Fukada S, Yamamoto Y, Yahagi H, Kanematsu M, Sato M, Ito T, Uezumi A, Hayashi S, Miyagoe-Suzuki Y, Takeda S, Tsujikawa K, Yamamoto H: Suppression of macrophage functions impairs skeletal muscle regeneration with severe fibrosis. Exp Cell Res 2008, 314:3232–3244
28. Grounds MD, McGeachie JK: A comparison of muscle precursor replication in crush-injured skeletal muscle of Swiss and BALBc mice. Cell Tissue Res 1989, 255:385–391
29. Gelman R, Watson A, Bronson R, Yunis E: Murine chromosomal regions correlated with longevity. Genetics 1988, 118:693–704
30. Lionikas A, Blizard DA, Vandenbergh DJ, Stout JT, Vogler GP, McClearn GE, Larsson L: Genetic determinants of weight of fast- and slow-twitch skeletal muscles in old mice. Mamm Genome 2006, 17:615–628
31. Heydemann A, Huber JM, Demonbreun A, Hadhazy M, McNally EM: Genetic background influences muscular dystrophy. Neuromuscul Disord 2005, 15:601–609
32. Manning EL, Crossland J, Dewey MJ, Van Zant G: Influences of

inbreeding and genetics on telomere length in mice. Mamm Genome 2002, 13:234–238
33. Kuang S, Kuroda K, Le Grand F, Rudnicki MA: Asymmetric self-renewal and commitment of satellite stem cells in muscle. Cell 2007, 129:999–1010
34. Schultz E, Lipton BH: Skeletal muscle satellite cells: changes in proliferation potential as a function of age. Mech Ageing Dev 1982, 20:377–383
35. Dykstra B, de Haan G: Hematopoietic stem cell aging and self-renewal. Cell Tissue Res 2008, 331:91–101
36. Chen J, Astle CM, Harrison DE: Genetic regulation of primitive hematopoietic stem cell senescence. Exp Hematol 2000, 28:442–450
37. Liang Y, Jansen M, Aronow B, Geiger H, Van Zant G: The quantitative trait gene latexin influences the size of the hematopoietic stem cell population in mice. Nat Genet 2007, 39:178–188
38. Sicinski P, Geng Y, Ryder-Cook AS, Barnard EA, Darlison MG, Barnard PJ: The molecular basis of muscular dystrophy in the mdx mouse: a point mutation. Science 1989, 244:1578–1580
39. Gargioli C, Coletta M, De Grandis F, Cannata SM, Cossu G: PIGF-MMP-9-expressing cells restore microcirculation and efficacy of cell therapy in aged dystrophic muscle. Nat Med 2008, 14:973–978
40. Muntoni F, Mateddu A, Marchei F, Clerk A, Serra G: Muscular weakness in the mdx mouse. J Neurol Sci 1993, 120:71–77
41. Hara H, Nolan PM, Scott MO, Bucan M, Wakayama Y, Fischbeck KH: Running endurance abnormality in mdx mice. Muscle Nerve 2002, 25:207–211
42. Carter GT, Wineinger MA, Walsh SA, Horasek SJ, Abresch RT, Fowler WM, Jr.: Effect of voluntary wheel-running exercise on muscles of the mdx mouse, Neuromuscul Disord 1995, 5:323–332
43. Lynch GS, Hinkle RT, Chamberlain JS, Brooks SV, Faulkner JA: Force and power output of fast and slow skeletal muscles from mdx mice 6–28 months old. J Physiol 2001, 535:591–600
44. Chamberlain JS, Metzger J, Reyes M, Townsend D, Faulkner JA: Dystrophin-deficient mdx mice display a reduced life span and are susceptible to spontaneous rhabdomyosarcoma. FASEB J 2007, 21:2195–2204

Acta Neuropathol (2010) 120:537–543
DOI 10.1007/s00401-010-0732-8

CASE REPORT

High-density areas on muscle CT in childhood-onset Pompe disease are caused by excess calcium accumulation

Keiko Ishigaki · Satomi Mitsuhashi · Ryohei Kuwatsuru · Terumi Murakami · Keiko Shishikura · Haruko Suzuki · Yoshito Hirayama · Ikuya Nonaka · Makiko Osawa

Received: 16 May 2010 / Revised: 15 July 2010 / Accepted: 24 July 2010 / Published online: 3 August 2010

Abstract We report two patients with childhood-onset Pompe disease showing striking changes with high-density areas on skeletal muscle CT, not seen in adult- or infantile-onset forms of this disease. While the anterior compartment of the thigh muscles was less affected in the adult-onset form, the rectus femoris and tibial muscles were preferentially involved from the early stage in the childhood-onset form of Pompe disease. The high-density areas became increasingly diffuse with disease progression, producing a marbled pattern and ultimately resulting in homogeneous high density and muscle atrophy. Muscle biopsy specimens from the high-density areas showed striking vacuolar changes with many dense globular bodies in lysosomes. High calcium signals were identified by X-ray microanalysis using energy-dispersive X-ray spectroscopy in these areas. Excess calcium accumulation in the vacuoles was also confirmed with the glyoxal-bis(2-hydroxyanil) (GBHA) staining. The high density on CT was slightly reduced together with clinical improvement after enzyme replacement therapy in patient 2. Our data demonstrate that in childhood-onset Pompe disease, high-density areas on skeletal muscle CT images are due to the accumulation of calcium in dense globular bodies formed by a chronic degenerative process affecting autophagic vacuoles.

Keywords Pompe disease · Childhood onset · High muscle CT density · Excess calcium accumulation · Enzyme replacement therapy

K. Ishigaki (✉) · T. Murakami · K. Shishikura · H. Suzuki · Y. Hirayama · M. Osawa
Department of Pediatrics, Tokyo Women's Medical University, School of Medicine, 8-1 Kawada-cho, Shinjuku-ku, Tokyo 162-8666, Japan
e-mail: keishi@ped.twmu.ac.jp

S. Mitsuhashi · I. Nonaka
National Center of Neurology and Psychiatry, Tokyo, Japan

R. Kuwatsuru
Department of Radiology, Tokyo Women's Medical University, School of Medicine, Tokyo, Japan

R. Kuwatsuru
Department of Radiology, Juntendo University, Faculty of Medicine, Tokyo, Japan

Introduction

Pompe disease is an autosomal recessively inherited disorder caused by a deficiency of the lysosomal enzyme acid alpha-glucosidase. It is classified into two major phenotypes, the infantile and late-onset forms, based on the time of disease onset [9]. The infantile form, originally described by Pompe, exhibits a rapidly progressive course characterized by prominent cardiomegaly, hepatomegaly, muscle weakness and hypotonia, and death before age 1 year. Late-onset Pompe disease is subdivided into childhood- and adult-onset forms. The childhood form usually presents with muscle weakness resembling that of progressive muscular dystrophy and is rarely associated with cardiomyopathy. Adult-onset Pompe disease is characterized by slowly progressive limb-girdle myopathy presenting as late as the second to sixth decade.

Computerized tomographic (CT) scanning of skeletal muscles is widely used for differential diagnosis or assessment of the progression of neuromuscular disorders [3, 12, 14]. The skeletal muscle CT abnormalities in adult-onset Pompe disease were reported to be atrophic, moth-eaten and washed-out changes in the paraspinal muscles [4]

and the vastus muscles of the thigh [5], and showed a pattern mimicking facioscapulohumeral dystrophy [10]. However, no report has summarized muscle CT findings in the childhood form. We previously reported a patient with childhood-onset Pompe disease showing high-density areas on CT in severely affected skeletal muscles [1]. Muscle biopsy of these high-density areas revealed pronounced vacuolar changes, while biopsy specimens from normal density areas had an essentially normal appearance. The second patient (patient 2) showed a very similar CT pattern, with high-density areas in the thigh and calf muscles, but no atrophic changes. In this study, we followed up CT changes in both the density and the volume of affected muscles in these two patients with age. We also determined whether the high-density areas improved with enzyme replacement therapy (ERT). Although the high-density areas on CT were associated with advanced vacuolar changes in muscle biopsy specimens, the precise mechanism whereby such changes were induced remains unknown. To clarify how CT density varies in the muscles of patients with Pompe disease, we analyzed this feature in the affected muscles.

Methods

Patients

Patient 1, previously reported elsewhere [1], was a 13-year-old boy at his first admission to our hospital. He had noticed muscle weakness and leg pain and severe headache upon awakening in the morning around 10 years of age. He had moderate muscle weakness only in the neck and trunk, without organomegaly. The characteristic histological findings and extremely low acid alpha-glucosidase activity (0.3 nmol 4 MU/mg/30 min, control: 7.3 ± 2.2) in biopsied muscle allowed a definitive diagnosis of Pompe disease. His genotype reflected compound heterozygous mutations, p.R600C and p.M439K, the former reportedly being common in Japanese patients. In his second decade, he suffered from repeated episodes of pneumothorax and respiratory infection. At age 19 years, non-invasive ventilation was necessitated by sudden aggravation of respiratory failure. He began ERT at 28 years but with no significant improvement and died of pneumonia at 29 years of age after 1 year treatment.

Patient 2 was an 11-year 3-month-old boy. At age 2 years, nasal voice became marked. He was apparently clumsy as compared with other children. At age 3 years, serum CK elevation to approximately 700 IU/l was detected incidentally during preoperative examination for nasopharyngeal incompetence. At age 5 years, he was diagnosed as having Pompe disease based on muscle biopsy findings and extremely low acid alpha-glucosidase activity, only 0.2 nmol 4 MU/mg/30 min (control: 7.3 ± 2.2). He had compound heterozygous missense mutations, p.S619R and p.E579K, which have already been reported. At 10 years and 3 months of age, International Charitable Access Program (ICAP) support allowed him to start ERT. At baseline, he could not jump and needed handrails to climb stairs. He was positive for Gowers' maneuver, and also had a waddling gait. He had mild respiratory failure and mild cardiac hypertrophy. ERT was initiated at a basic dosage of 20 mg/kg. Six months after starting ERT, his respiratory and motor functions were markedly improved.

Bone density was normal with normal renal function. Serum calcium levels and urine calcium to creatinine ratios (Ca/Cr) were within normal limits, measuring 8.8 mg/dl (normal 8.5–9.9) and 0.04 mg/mg (normal < 0.20) in patient 1 and 9.4 mg/dl and 0.02 mg/mg in patient 2, respectively. Serum phosphate and magnesium levels were also within normal limits, measuring 3.9 mg/dl (normal 2.5–4.5 mg/dl) and 1.5 mEq/l (normal 1.2–2.0) in patient 1 and 4.5 mg/dl and 1.5 mEq/l in patient 2, respectively. None of the patients had any abnormal symptoms of calcium metabolism. There was no clinical difference between our patients and others with the childhood form: all had proximal dominant progressive muscular weakness, respiratory dysfunction and slightly elevated CK levels.

Skeletal muscle CT scans

Skeletal muscle CT scans were obtained at seven levels, i.e., shoulder, mid-upper arm, mid-forearm, 3rd lumbar vertebra, pelvic girdle, mid-thigh and mid-calf (Hitachi CT 600 scanner, CT W-200, GE Highspeed Advantage SG, and Toshiba Aquilion 4 Detector). The scanning conditions, identical at all times, were 120 kVp, 150 mA and 0.5 ms. The CT number setting in Hounsfield units (HU) gives water a value of zero, air a value of −1,000 and bone a value of +1,000. The CT imaging should be displayed in the grey scales by adjusting window level (WL) and window width (WW) depending on target organs. The WW switch selects the range of absorption values that determine black and white on the display. The WL control enables the center of the range selected by the WW switch to be set at any desired point in the system's scale between −1,000 and +1,000. The earlier scans were obtained at a WL of 25 HU and WW of 225 HU using a Hitachi CT 600 scanner to evaluate skeletal muscles, while the more recent scans were obtained at WL 30–45 HU and WW 300–350 HU with more advanced CT scanners. Patient 1 was assessed at age 13, 22 and 29, and patient 2 at 5 and 10 years of age.

We also examined muscle CT on two patients with the infantile-onset, three with adult-onset forms and a 10-year-old girl with McArdle disease under the same conditions for comparison.

Morphological analysis

Biopsy specimens were taken from the rectus femoris, which showed high-density areas on CT, in both patients and from the vastus lateralis showing normal density in patient 1 at age 13 years (Fig. 5a). As a disease control, we selected two representative muscle biopsies from a patient with the infantile-onset form and two from another with the adult-onset form. Staining, including hematoxylin and eosin (HE) stain and Periodic acid-Schiff (PAS) stain, was performed by standard procedures. We also applied glyoxal-bis(2-hydroxyanil) (GBHA) staining to demonstrate insoluble red precipitates of calcium (Ca)–GBHA complexes in the muscle biopsy specimens. McArdle disease has abnormal glycogen metabolism but with small amount of glycogen accumulation and absent autophagic phenomenon. To confirm whether abnormal glycogen metabolism itself induces calcium accumulation in muscle fibers, we selected a 10-year-old patient with the McArdle disease as a disease control, and 20 normal muscles as healthy controls.

X-ray microanalysis (S-5200 ultra resolution scanning electron microscope: HITACHI)

The rectus femoris muscle was fixed in phosphate-buffered 2.5% glutaraldehyde, post-fixed in 1.5% osmium tetroxide and then embedded in epoxy resin employing a standard procedure. The sample was sectioned at approximately 0.1 μm and analyzed at 20 kV with an S-5200 ultra resolution scanning electron microscope (HITACHI) using the energy-dispersive X-ray spectroscopy (EDX) method. Samples from patients with juvenile dermatomyositis and Duchenne muscular dystrophy were analyzed for comparison.

Results

Skeletal muscle images

Both patients with the childhood-onset form specifically showed high-density areas on CT in the rectus femoris and tibialis anterior muscles from the early stage (Figs. 1a–c, 2a, b). The CT number (attenuation) for the high-density areas was approximately 130 HU, while these were in the 30–40 HU range in healthy controls. Even in the areas with near-normal density, CT numbers were increased to 70–80 HU in both patients. The skeletal muscle CT numbers in the patient with McArdle disease were slightly increased to 50–60 HU in all areas examined.

In patient 1 at 13 years of age, high-density areas were localized in the rectus femoris, as well as small portions of the adductor magnus and anterior tibialis muscles (Fig. 1b, c). The high-density areas became more diffuse with age, resulting in a marbled pattern but neither showed moth-eaten nor washed-out changes (Fig. 1e, f). Ultimately, most of his thigh and calf muscles showed homogeneous high density with marked volume loss (Fig. 1h, i). The paraspinal and iliopsoas muscles were also affected but there were no high-density areas (Fig. 1g).

In patient 2 at age 5 years, the rectus femoris muscle was mildly affected and high-density areas were detectable in the tibialis anterior and peroneal muscles (Fig. 2a, b). At 10 years of age, high-density areas became evident in the rectus femoris and also appeared in the vastus lateralis and gracilis muscles (Fig. 2c, d). He showed marked improvement of motor and respiratory functions 3 months after starting ERT. He could jump and climb stairs unaided. The CT numbers, of which the maximum had been 138 HU and the minimum 88 HU (138/88) at the beginning of ERT (Fig. 2c, d), improved slightly to 100/64 HU after

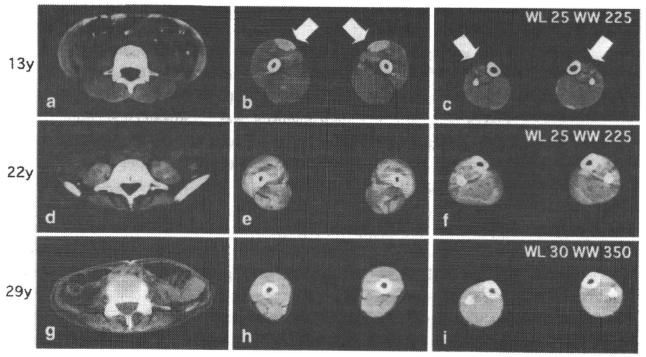

Fig. 1 Skeletal muscle CT scans in patient 1 at 13 years (**a–c**), 22 years (**d–f**) and 29 years (**g–i**) of age. Note high-density areas (*arrows*) in rectus femoris (**b**) and milder findings in the tibialis anterior (**c**) muscles, relatively sparing the posterior compartment of the thigh and calf muscles. As the high-density areas became more diffuse, a marbled pattern (**e**, **f**) appeared and eventually involved all leg muscles (**h**, **i**). Paraspinal muscles are also involved but do not show high-density areas (**a**, **d**, **g**). *WL* window level, *WW* window width of CT scanning

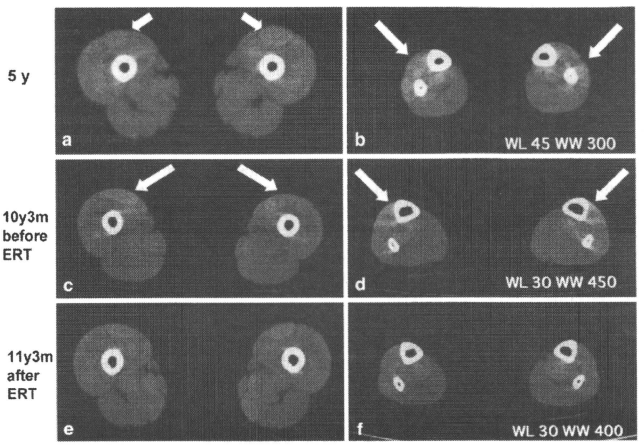

Fig. 2 Skeletal muscle CT scans in patient 2 at 5 years (**a**, **b**), 10 years (before ERT) (**c**, **d**) and 11 years (1 year after starting ERT) (**e**, **f**) of age. The rectus femoris (*arrows*) is only mildly affected, with no high-density areas (**a**), while the tibialis anterior (*arrows*) and peroneal muscles are more significantly involved and show high-density areas at age 5 years (**b**). Note evident high-density areas (*arrows*) in the rectus femoris at age 10 years (**c**). The high-density areas on CT were slightly reduced together with clinical improvement after ERT (**e**, **f**)

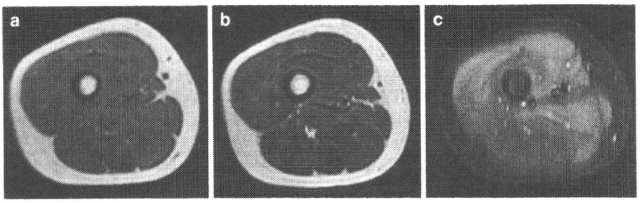

Fig. 3 Skeletal muscle MR images in patient 2 at 10 years of age. Very mildly increased intensity was recognized in the rectus femoris and adductor magnus on T1-weighted image (**a**). There was no detectable marked change on T2-weighted image (**b**). The high intensity was most clearly demonstrated in fat suppression on T1-weighted image (**c**)

4 months of this treatment, but they had returned to the original levels of 136/77 HU at 8 months and 140/80 at 1 year after starting ERT (Fig. 2e, f).

For comparison, we examined muscle MRI in patient 2 at 10 years of age (Fig. 3). Very mildly increased intensity was recognized in the rectus femoris and adductor magnus on T1-weighted images (Fig. 3a). The high intensity was more clearly demonstrated on fat suppression T1-weighted MRI (Fig. 3c) similar to that on CT. There was no marked change on T2-weighted images (Fig. 3b).

Morphological analysis

As we reported previously [1], histopathological findings were consistent with CT findings, i.e., the rectus femoris with extremely high-density areas on CT had numerous vacuoles filled with large amounts of glycogen (Fig. 5b), while the vastus lateralis muscles with normal CT density had a nearly normal appearance with few vacuoles (Fig. 5c) [1].

X-ray microanalysis with energy-dispersive X-ray spectroscopy (EDX) is an analytical technique used for elemental analysis of samples. In our patients' muscles, a mildly elevated Ca signal was detected in an area with glycogen accumulation (Fig. 4a, b), especially in electron dense globular bodies in vacuoles (Fig. 4c, d). As to disease controls, a low Ca signal was demonstrated in a few areas in a case with Duchenne muscular dystrophy, but none in muscles affected by dermatomyositis.

To demonstrate Ca deposition histochemically, we stained muscle biopsy specimens by the GBHA method in which insoluble red precipitates of Ca-GBHA complexes form under conditions of high Ca deposition. Nearly all of the fibers with vacuoles, in the specimens from the high-density areas on CT, were strongly reactive for GBHA (Fig. 5d),

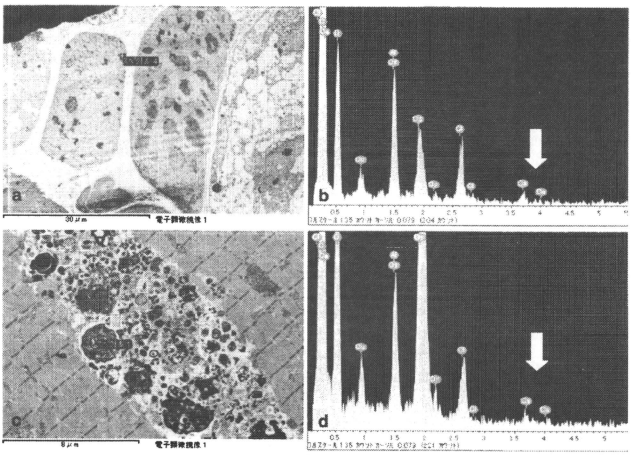

Fig. 4 X-ray microanalysis at 15 kV on an area (*arrow*) of excess glycogen accumulation (**a**) showed high Ca signals (**b**). At the electron dense globular bodies (*arrow*) (**c**), Ca signals were significantly elevated (**d**). **a**, **b** Electron micrographs from patient 2

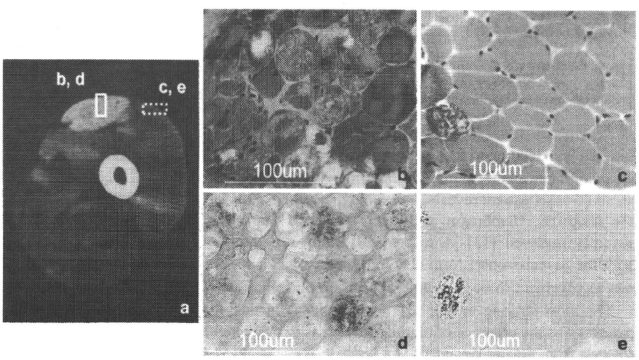

Fig. 5 Ca accumulation in rectus femoris muscles with high-density (*marked by solid line*) areas (**b**, **d**) and the vastus lateralis with normal CT density (*marked by dashed line*) (**c**, **e**) in the skeletal muscle CT scan (**a**) in patient 1 at 13 years of age. Numerous vacuoles filled with dense granular material (**b**) are strongly stained with GBHA (**d**) indicating increased amounts of Ca in the dense bodies. Note a few vacuolated fibers with calcium deposition in the less affected vastus lateralis muscle (**c**, **d**). **b**, **c** Hematoxylin and eosin staining, **d**, **e** GBHA staining

while GBHA reactions were localized in only a few affected fibers in muscles with normal density (Fig. 5e). GBHA positivity was not prominent in our two patients with the infantile-onset form or the two with the adult-onset form of Pompe disease. When we applied PAS staining to epon-embedded sections, dense globular bodies were strikingly prominent in the childhood form (Fig. 6a) but in neither the infantile- (Fig. 6b) nor the adult-onset form.

Discussion

In late-onset Pompe disease, including the childhood- and adult-onset forms, the most common feature is skeletal and respiratory muscle involvement sparing cardiac muscle. Whether the distribution-affected muscle differs between the two late-onset forms remains an open question. As observed in our patients, the anterior compartment of thigh muscles is preferentially involved in the childhood-onset form, and posterior thigh and truncal muscles in the adult-onset form [4, 5]. The affected muscles in the adult-onset form are atrophic with a moth-eaten, washed-out appearance. One report emphasized truncal muscle involvement mimicking that of facioscapulohumeral dystrophy [10].

Muscle MRI done on 11 patients with the adult-onset form [11] also demonstrated the posterior compartment of the thigh, including the adductor magnus and semimembranous muscles, to be affected from the early stage

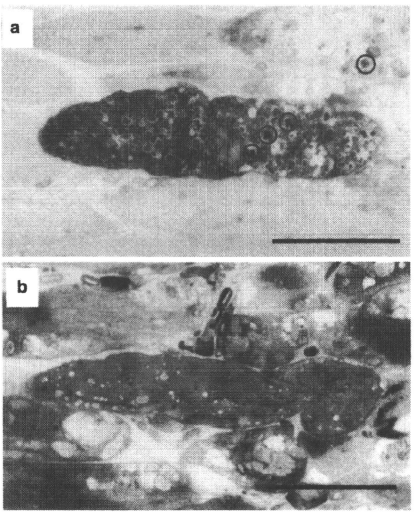

Fig. 6 Epon-embedded sections stained with PAS. Note that dense globular bodies (*circled*) in lysosomes are more prominent in the childhood-onset (**a**) than in infantile-onset (**b**) form. *Bar* 100 μm

ultimately extending to the long head of the biceps femoris, semitendinous and then anterior thigh muscles. Autopsy of an adult-onset patient revealed proximal muscles, including the iliopsoas, diaphragm and intercostals, to be most severely involved [13]. A recent MRI study on siblings with the juvenile-onset form also indicated adductor magnus involvement to be the earliest manifestation [6].

The most striking muscle CT abnormality seen in our patients was the presence of high-density areas in the rectus femoris from the early stage of this disease. These changes became increasingly prominent with age. High-density areas on CT scans have already been recognized as being consistent with the severity of pathological change, but the cause of these high-density changes remains uncertain. In patient 1, the high-density areas persisted into the third decade. Such high-density areas have not previously been documented in other myopathic disorders, including inflammatory myopathies and muscular dystrophies. Increased CT density has been described in glycogen-laden organs in various glycogen storage disorders including von Gierke's disease [2, 7, 8]. Glycogen solution reportedly exhibits an attenuation coefficient increase of 2.5–3.0 HU with each 1% increase in glycogen concentration in vitro [8]. Thus, excess glycogen itself can explain the increased CT density in patients with glycogen storage disorders.

Since the CT density in our patients was too high to simply reflect increased amounts of glycogen, we speculated that there were additional factors related to autophagic vacuoles, especially the end-products of autophagocytosis. It is well known that bleeding and calcification increase CT density. Therefore, we conducted X-ray microanalyses to identify the elements responsible for the observed density increases. This technique allows identification and assay of elements contained in samples by analyzing element-specific X-rays. Employing this method, we found high Ca signals in muscle specimens, especially in electron dense globular bodies in autophagic vacuoles. The strong GBHA staining also supports the concept of excess Ca accumulation in autophagic vacuoles. Therefore, Ca accumulation in autophagic vacuoles, rather than glycogen, appears to be the source of high-density areas in skeletal muscle on CT in childhood-onset Pompe disease patients. The mildly elevated intensity on T1-weighted images which was more clear on fat suppression on T1-weighted skeletal muscle MRI also supports calcification, rather than fatty replacement as in the adult-onset form. As shown in this patient, the muscle CT is much more informative than MRI for some disorders, especially chronic myopathies with calcification.

In muscular dystrophies, the hypercontracted fibers sometimes show high calcium accumulation. Since calcium in such fibers is soluble, the staining pattern is rather uniform which is quite different from granular pattern seen in the present biopsies. In other autophagic myopathies with rimmed vacuole formation and Danon disease, calcium accumulation was not found on GBHA staining (personal observation by Dr Nonaka).

Calcium accumulation in dense globular bodies in the lysosomes was confirmed by X-ray microanalysis and GBHA staining; however, its mechanism is not fully understood. Those dense bodies were not prominent in the infantile- and adult-onset forms. Since it may take some time to form dense globular bodies, probably via chronic degeneration of undigested glycogen particles in lysosomes, muscle degeneration may be too rapid to form such inclusion bodies with Ca accumulation in the infantile form. In the adult form, glycogen accumulation in the lysosomes and vacuolar formation are limited; therefore, calcium accumulation is not prominent. It is therefore quite reasonable that these high-density CT areas on CT are prominently seen in the childhood form, but not in other forms of Pompe disease.

Our findings came from only two patients, still we know that there are other Japanese patients with childhood-onset Pompe disease who show the exact same results such as high-density areas on skeletal muscle CT (personal communications). Study of a larger cohort will be helpful to confirm our hypothesis.

Acknowledgments This study was supported by the Research Grant (21B-12) for Nervous and Mental Disorders from the Ministry of Health, Labour and Welfare. The authors thank Drs. Hideo Sugie and Tokiko Fukuda, Jichi Children's Medical Center Tochigi, Jichi Medical University, for the biochemical analysis, Dr. Hiroshi Kobayashi, The Jikei University School of Medicine, Drs. Torayuki Okuyama and Eri Oda, National Center for Child Health and Development for the genetic analysis and Rieko Takahashi for technical assistance. We also thank Dr. Kayoko Saito, Institute of Medical Genetics, Tokyo Women's Medical University and Dr. Mitsuru Kawai, Higashi-Saitama National Hospital for clinical advice.

References

1. Arai Y, Osawa M, Shishikura K et al (1993) Computed tomography and magnetic resonance imaging of affected muscle in childhood acid alpha-glucosidase deficiency. Brain Dev 15:147–152
2. Biondetti PR, Fiore D, Muzzio PC (1980) Computed tomography of the liver in von Gierke's disease. J Comput Assist Tomogr 5:685–686
3. Calò M, Crisi G, Martinelli C, Colombo A, Schoenhuber R, Gibertoni M (1986) CT and the diagnosis of myopathies-preliminary findings in 42 cases. Neuroradiology 28:53–57
4. Cinnamon J, Slonim AE, Black KS, Gorey MT, Scuderi DM, Hyman RA (1991) Evaluation of the lumbar spine in patients with glycogen storage disease: CT demonstration of patterns of paraspinal muscle atrophy. Am J Neuroradiol 12:1099–1103
5. de Jager AEJ, van der Vilet TM, van der Ree TC, Oosterink J, Loonen MCB (1998) Muscle computed tomography in adult-onset acid maltase deficiency. Muscle Nerve 21:398–400
6. Dlamini N, Jan W, Norwood F et al (2008) Muscle MRI findings in siblings with juvenile-onset acid maltase deficiency (Pompe disease). Neuromuscul Disord 18:408–409
7. Doppman JL, Cornblath M, Dwyer AJ, Adams AJ, Girton ME, Sidbury J (1982) Computed tomography of the liver and kidneys in glycogen storage disease. J Comput Assist Tomogr 6:67–71
8. Dweyer A, Doppman JL, Adams AJ, Girton ME, Chernick SS, Cornblath M (1983) Influence of glycogen on liver density: computed tomography from a metabolic perspective. J Comput Assist Tomogr 7:70–73
9. Engel AG, Hirschhorn R, Huie ML (2004) Acid maltase deficiency. In: Engel AG, Franzini-Armstrong C (eds) Myology, vol 2, 3rd edn. McGraw Hill, New York, pp 1559–1580
10. Ohya Y, Morita H, Ogawa M, Nonaka I, Tsujino S, Kawai M (2001) A case of adult-onset acid maltase deficiency with affected muscles patterns resembling FSHD. Rinsho-Shinkei 41:390–396 (in Japanese)
11. Pichiecchio A, Uggetti C, Ravaglia S et al (2004) Muscle MRI in adult-onset acid maltase deficiency. Neuromuscul Disord 14:51–55
12. Swash M, Brown MM, Thakkar C (1995) CT muscle imaging and the clinical assessment of neuromuscular disease. Muscle Nerve 18:708–714
13. Van der Walt JD, Swash M, Leake J, Cox EL (1987) The pattern of involvement of adult-onset acid maltase deficiency at autopsy. Muscle Nerve 10:272–281
14. Vliet AM, Thijssen HOM, Joosten E, Merx JL (1988) CT in neuromuscular disorders: a comparison of CT and histology. Neuroradiology 30:421–425